

Balancing the Cosmic Energy Budget: The Cosmic X-ray Background, Blazars, and the Compton Thick AGN Fraction

A. R. Draper and D. R. Ballantyne

*Center for Relativistic Astrophysics, School of Physics, Georgia Institute of Technology,
Atlanta, GA 30332*

aden.draper@physics.gatech.edu

ABSTRACT

At energies $\gtrsim 2$ keV, active galactic nuclei (AGN) are the source of the cosmic X-ray background (CXB). For AGN population synthesis models to replicate the peak region of the CXB (~ 30 keV), a highly obscured and therefore nearly invisible class of AGN, known as Compton thick (CT) AGN, must be assumed to contribute nearly a third of the CXB. In order to constrain the CT fraction of AGN and the CT number density we consider several hard X-ray AGN luminosity functions and the contribution of blazars to the CXB. Following the unified scheme, the radio AGN luminosity function is relativistically beamed to create a radio blazar luminosity function. An average blazar spectral energy density model is created to transform radio luminosity to X-ray luminosity. We find the blazar contribution to the CXB to be 12% in the 0.5-2 keV band, 7.4% in the 2-10 keV band, 8.9% in the 15-55 keV band, and 100% in the MeV region. When blazars are included in CXB synthesis models, CT AGN are predicted to be roughly one-third of obscured AGN, in contrast to the prediction of one half if blazars are not considered. Our model implies a BL Lac X-ray duty cycle of $\sim 13\%$, consistent with the concept of intermittent jet activity in low power radio galaxies.

Subject headings: galaxies: active — galaxies: jets — galaxies: quasars: general — X-rays: diffuse background

1. Introduction

Nearly half a century after the cosmic X-ray background (CXB) was discovered (Giacconi et al. 1962), the majority of the CXB up to 10 keV has been resolved into distinct point sources by

deep observations conducted by *ROSAT*, *Chandra*, and *XMM-Newton* (Hasinger et al. 1998; Mushotzky et al. 2000; Giacconi et al. 2001, 2002; Hasinger et al. 2001; Alexander et al. 2003; Worsley et al. 2004; Brandt & Hasinger 2005; Worsley et al. 2005). These discrete sources are active galactic nuclei (AGN), compact extra-galactic sources powered by accretion onto black holes (Lyndon-Bell 1969; Rees 1984). As such, the CXB encapsulates the history of accretion onto super massive black holes and provides a powerful tool to aid scientific understanding of accretion processes (Fabian & Barcons 1992). It has been shown that a large portion of this accretion is shrouded from our view by intervening matter along the line of sight (Setti & Woltjer 1989; Celotti et al. 1992; Madau et al. 1994; Comastri et al. 1995; Fiore et al. 1999; Treister et al. 2009). For AGN spectral and spatial density models to match the peak of the CXB at ~ 30 keV, the models must predict a large number of highly obscured sources known as Compton thick (CT) AGN (Risaliti et al. 1999; Ueda et al. 2003; Treister & Urry 2005; Ballantyne et al. 2006; Gilli et al. 2007), which have a neutral hydrogen column density $N_{\text{H}} \gtrsim 1.5 \times 10^{24} \text{ cm}^{-2}$ (Treister et al. 2009), making them practically invisible in the 2-10 keV band (Ghisellini et al. 1994). CXB synthesis models predict CT sources make up roughly half of the obscured AGN population (Risaliti et al. 1999; Ueda et al. 2003; Treister & Urry 2005; Ballantyne et al. 2006; Gilli et al. 2007).

In recent years, studies to observationally constrain the CT fraction have been undertaken. At first, small local studies seemed to agree with the model predictions that half of all obscured AGN are CT (Risaliti et al. 1999; Guainazzi et al. 2005). However, a recent study by Treister et al. (2009), using samples from *INTEGRAL* and *Swift* observations and high redshift, IR-selected CT AGN candidates, suggests that CT AGN contribute only about 9% of the X-ray background, which contrasts sharply to the prediction by Gilli et al. (2007) that CT AGN account for nearly a third of the CXB. Malizia et al. (2009) studied 88 AGN observed by *INTEGRAL/IBIS* in the 20-40 keV band and found that at least 16% of obscured AGN are CT and $\gtrsim 24\%$ of the AGN in their local sample ($z \leq 0.015$) are CT. If $\sim 75\%$ of local AGN are obscured (Risaliti et al. 1999; Treister et al. 2009), the local AGN sample of Malizia et al. (2009) suggests that $\gtrsim 32\%$ of obscured AGN are CT. Given the uncertainty of the CT AGN fraction, smaller classes of CXB contributors must be considered. The CXB contribution from the small class of AGN known as blazars has previously been ignored by CXB synthesis models and CT AGN fraction predictions, even though blazars are known to emit in a broad range from radio to TeV energies. To further constrain model predictions of the CT AGN fraction, the blazar class of AGN must be considered.

Blazars are a unique and extreme class of AGN. Unified models of AGN, as summarized by Antonucci (1993) and Urry & Padovani (1995), explain blazars as radio galaxies with relativistic jets viewed close to the line of sight. Flat spectrum radio quasars (FSRQs) are relativistically beamed FRIIs (luminous radio galaxies) and BL Lac objects (BL Lacs)

are relativistically beamed FRIs (less luminous radio galaxies). The features which define blazars (extreme variability, high luminosity, high polarization, and radio core-dominance) are due to the relativistic beaming caused by looking down the relativistic jet of the blazar (Padovani et al. 2007). The details of the spectral energy distribution (SED) of blazars is still a topic riddled with uncertainties (Kneiske & Mannheim 2008). The extreme variability that distinguishes the blazar class necessitates simultaneous multi-wavelength observations to understand the spectral properties (Ghisellini & Tavecchio 2008). However, the two-hump form of the blazar SED, spanning from radio to γ -ray energies, is well known (Urry 1999). The lower energy hump is due to synchrotron radiation while the higher energy hump is due to inverse Compton scattering (Urry & Padovani 1995). It has been shown that blazars are significant progenitors of the γ -ray background (Giommi et al. 2006; Narumoto & Totani 2006; Kneiske & Mannheim 2008); therefore it is expected that blazars should have a non-negligible contribution to the CXB.

Giommi et al. (2006) predict that blazars should account for 11-12% of the soft CXB around 1 keV; however, no estimation is made for the blazar contribution to the peak region of the CXB around 30 keV. A recent study by Ajello et al. (2009), based on the three year *Swift*/BAT blazar sample, claims that blazars contribute about 10% of the X-ray background in the 2-10 keV band. In the 15-55 keV band Ajello et al. (2009) predict blazars contribute $\sim 20\%$ if blazars are modeled as a single population or $\sim 9\%$ if FSRQs and BL Lacs are modeled as two distinct populations. Both Giommi et al. (2006) and Ajello et al. (2009) found that blazars could contribute 100% of the CXB in the MeV band.

Due to uncertainties in the low luminosity end of the AGN hard X-ray luminosity function (HXLF), multiple HXLFs must be considered (e.g., Ueda et al. 2003; La Franca et al. 2005; Silverman et al. 2008; Aird et al. 2009; Ebrero et al. 2009; Yencho et al. 2009) to understand the range of predicted CT AGN. Recent AGN HXLFs find that luminosity-dependent density evolution (LDDE) provides the best fit to the observational data (Ueda et al. 2003; Hasinger et al. 2005; La Franca et al. 2005; Silverman et al. 2008; Ebrero et al. 2009; Yencho et al. 2009). Aird et al. (2009) find a new evolutionary model, luminosity and density evolution (LADE), also fits the observational data well. Both the LDDE and LADE models are in keeping with the findings that the scarce, high-luminosity sources, quasars, show sharp positive evolution from $z \approx 0-2$, while less luminous sources, Seyferts, evolve more temperately (Barger et al. 2005; Brandt & Hasinger 2005; Hasinger et al. 2005). Given the connection between AGN and galaxy evolution (e.g., Ferrarese & Merritt 2000; Smolčić 2009), it is not surprising that AGN evolution matches the trend of galaxy formation, where massive galaxies formed earlier in cosmological time while smaller structures have waited until more recent times to form (e.g., Cowie et al. 1999).

In this work the blazar contribution to the CXB is predicted and the implications for the CT AGN fraction are discussed in the context of multiple HXLFs. In §2 we present the model used for the blazar and non-blazar AGN contributions to the CXB. In §3 our results are presented while discussions and conclusions are given in §4. We assume a Λ CDM cosmology with $H_0 = 70 \text{ km s}^{-1} \text{ Mpc}^{-1}$, $\Omega_\Lambda = 0.7$, and $\Omega_m = 0.3$ (Spergel et al. 2007).

2. Calculations

2.1. Blazar Contribution to X-ray Background

2.1.1. Luminosity Function

The widely accepted unified scheme of radio loud AGN is that FSRQs are FRIIs, luminous radio galaxies, with jets pointed along the line of sight causing the observed radiation to be relativistically beamed, and that BL Lacs have an analogous relationship with FRIs, less luminous radio galaxies (Urry & Padovani 1995). Thus, the blazar luminosity function, which describes blazar space density and evolution, should be well represented by the relativistically beamed radio galaxy luminosity function (Urry et al. 1991; Padovani & Urry 1992; Padovani et al. 2007).

Willott et al. (2001) represent the radio galaxy luminosity function as the sum of the low and high luminosity radio galaxies. The luminosity function is of the form

$$\frac{d\Phi(L_{151\text{MHz}}, z)}{d \log L_{151\text{MHz}}} = \frac{d\Phi_l(L_{151\text{MHz}}, z)}{d \log L_{151\text{MHz}}} + \frac{d\Phi_h(L_{151\text{MHz}}, z)}{d \log L_{151\text{MHz}}} \quad (1)$$

where

$$\frac{d\Phi_l(L_{151\text{MHz}}, z)}{d \log L_{151\text{MHz}}} = \rho_{l0} \left(\frac{L}{L_{l*}} \right)^{-\alpha_l} \exp \left(-\frac{L}{L_{l*}} \right) f_l(z) \quad (2)$$

and

$$\frac{d\Phi_h(L_{151\text{MHz}}, z)}{d \log L_{151\text{MHz}}} = \rho_{h0} \left(\frac{L}{L_{h*}} \right)^{-\alpha_h} \exp \left(-\frac{L_{h*}}{L} \right) f_h(z), \quad (3)$$

where $L_{151\text{MHz}}$ is the monochromatic luminosity at 151 MHz.

Willott et al. (2001) use three different evolutionary models for $f_h(z)$, which differ by the evolutionary scenerio for high luminosity radio galaxies for $z \gtrsim 2$. Model A assumes a symmetric evolutionary scenerio where the density of high luminosity radio galaxies postively evolves until $z \sim 2$ and then evolves negatively at the same rate for $z \gtrsim 2$. Model B assumes a postive evolution up to $z \sim 2$ and no evolution beyond $z \sim 2$. Model C assumes positive evolution of high luminosity radio galaxies up to $z \sim 2$ and for $z \gtrsim 2$ negative evolution is

assumed, however the negative evolution is not assumed to be symmetric with respect to $z \sim 2$. Due to the lack of high redshift sources in the sample used by Willott et al. (2001), all three models fit the data well. Model C is used here as it is the most general scenerio. The Willott luminosity function is converted from Einstein-de Sitter cosmology to Λ CDM cosmology.

To relate the parent luminosity function to the beamed luminosity function we use the procedure laid out by Urry & Shafer (1984) and Urry & Padovani (1991). The beamed luminosity L is assumed to be related to the rest frame luminosity \mathcal{L} by

$$L = (1 + f\delta^p) \mathcal{L}, \quad (4)$$

where f is the fraction of the unbeamed luminosity that is relativistically beamed by the jet, and $\delta = [\gamma(1 - \beta \cos \theta)]^{-1}$ is the jet Doppler factor with β the apparent velocity in units of c , the speed of light. Finally, $\gamma = (1 - \beta^2)^{-\frac{1}{2}}$ is the Lorentz factor, and θ is the angle between the stream of the jet and the line of sight. The exponent p is defined as $p = 3 + \alpha$ for continuous jets and $p = 2 + \alpha$ for discrete jets, where α is the spectral index, and accounts for aberration, time contraction, and the blue-shifting of the photons (Urry & Shafer 1984). The probability of observing luminosity L given unbeamed luminosity \mathcal{L} is

$$P_\gamma(L|\mathcal{L}) = \frac{1}{\beta\gamma p} f^{1/p} \mathcal{L}^{-1} \left(\frac{L}{\mathcal{L}} - 1 \right)^{-(p+1)/p}. \quad (5)$$

The luminosity function for a particular Lorentz factor $d\Phi_\gamma/d\log L$ is found by integrating the intrinsic differential luminosity function $d\Phi_e/d\log L$ such that

$$\frac{d\Phi_\gamma(L)}{d\log L} = \int d\mathcal{L} \frac{d\Phi_e(\mathcal{L})}{d\log \mathcal{L}} \frac{d\log \mathcal{L}}{d\log L} P_\gamma(L|\mathcal{L}). \quad (6)$$

To accommodate a range of Lorentz factors, we define the Lorentz factor distribution $n(\gamma)$ so $n(\gamma) \propto \gamma^G$ and is normalized to one over the full range of Lorentz factors. Thus the observed blazar luminosity function $d\Phi_o/d\log L$ is

$$\frac{d\Phi_o(L)}{d\log L} = \int d\gamma \frac{d\Phi_\gamma(L)}{d\log L} n(\gamma). \quad (7)$$

By performing this procedure for L and \mathcal{L} pairings allowed by $0 \leq \theta \leq \theta_c$, where θ_c is defined by $f\delta(\theta_c)^p \equiv 1$ (Urry & Padovani 1991) the angle at which the beamed jet luminosity is equal to the intrinsic luminosity, we construct the luminosity function for the population of radio galaxies which have spectra dominated by relativistic beaming.

To construct the blazar luminosity function the low luminosity function $d\Phi_l/d\log L_{151MHz}$, defined by equation 2, is set as the parent luminosity function for BL Lac objects and the

high luminosity function $d\Phi_h/d\log L_{151\text{MHz}}$, defined by equation 3, is set as the parent luminosity function for FSRQs. Above $L_{151\text{MHz}} \approx 10^{43.8} \text{ erg s}^{-1}$ or $L_{151\text{MHz}} \approx 10^{27.1} \text{ W Hz}^{-1}$, at $z = 0$, the luminosity function is dominated by FSRQs and below this point the BL Lac luminosity function is dominant. For BL Lacs $p = 3 + \alpha = 2.7$ (Urry et al. 1991), and for FSRQs $p = 3 + \alpha = 2.9$ (Padovani & Urry 1992). To determine f and G , an average viewing angle and average Lorentz factor is selected in agreement with those found by Hovatta et al. (2009). For BL Lacs the average viewing angle is 5.5° and average Lorentz factor is 10.3 and for FSRQs the average viewing angle is 4.4° and average Lorentz factor is 16.2. The range of Lorentz factors for both BL Lacs and FSRQs is $5 \leq \gamma \leq 40$ (Padovani & Urry 1992) and the range of intrinsic luminosities (in erg s^{-1}) is $39.5 \leq \log L_{151\text{MHz}} \leq 47.5$ (Smolčić et al. 2009; Ajello et al. 2009). The results are not sensitive to the limits of integration as long as for the lower limit $\log L_{151\text{MHz}}^{\min} \lesssim 40.0$ and for the upper limit $\log L_{151\text{MHz}}^{\max} \gtrsim 45.5$. The FSRQ (solid line) and BL Lac (dashed line) luminosity functions at $z = 1$ are shown in Figure 1.

2.1.2. Formalism

We follow the formalism laid out in previous works (e.g., Comastri et al. 2005; Pompilio et al. 2000; Ballantyne et al. 2006) to compute the extragalactic background spectrum due to AGN and blazars and the associated number counts. The spectral intensity at X-ray or γ -ray energy E due to blazars is given by

$$I(E) = \frac{c}{H_0} \int_{z_{\min}}^{z_{\max}} \int_{\log L_{151\text{MHz}}^{\min}}^{\log L_{151\text{MHz}}^{\max}} \frac{d\Phi(L_{151\text{MHz}}, z)}{d\log L_{151\text{MHz}}} \frac{S_E(L_{151\text{MHz}}, z) d_l^2}{(1+z)^2 [\Omega_m(1+z)^3 + \Omega_\Lambda]^{1/2}} d\log L_{151\text{MHz}} dz, \quad (8)$$

where $d\Phi(L_{151\text{MHz}}, z)/d\log L_{151\text{MHz}}$ is the blazar luminosity function at 151 MHz (in units of Mpc^{-3}), $S_E(L_{151\text{MHz}}, z)$ is the observed spectrum at energy E (in units of $\text{keV cm}^{-2} \text{ s}^{-1} \text{ keV}^{-1}$) for a blazar with intrinsic 151 MHz luminosity $L_{151\text{MHz}}$ at redshift z , and d_l is the luminosity distance of redshift z . A similar method is used to calculate the number counts within a specified energy band as shown by Ballantyne et al. (2006) equation 3.

2.1.3. Spectrum

Blazars have a distinct spectral shape characterized by two bumps, a synchrotron peak and a higher frequency inverse Compton (IC) peak. The ‘Blazar Sequence’, in which the spectrum of a blazar can be uniquely determined based solely on the bolometric luminosity of the blazar (Fossati et al. 1997, 1998; Ghisellini et al. 1998; Donato et al. 2001) was considered as a blazar SED model; however, the anti-correlation between the synchrotron

peak frequency and the synchrotron peak luminosity has been proposed to be due to sample selection effects (Caccianiga & Marchã 2004; Padovani 2007; Ghisellini & Tavecchio 2008) and possibly variable Doppler boosting (Nieppola et al. 2008). A ‘new Blazar Sequence’ has been proposed which parametrizes the blazar SED by the black hole mass and the accretion rate (Ghisellini & Tavecchio 2008); however, the new Blazar Sequence still predicts an anti-correlation between the synchrotron peak frequency and synchrotron peak luminosity (Nieppola et al. 2008).

As there is no widely accepted blazar SED model, the blazar population was split into three subclasses (FSRQs, Low-peaked BL Lacs (LBL), and High-peaked BL Lacs (HBL)) and SED models were created for each subclass based on well sampled spectra of subclass members. Details of the SED parametrization can be found in Appendix A. For each subclass we set the synchrotron peak frequency, ν_S , the IC peak frequency, ν_{IC} , and the relative luminosity of the synchrotron and IC peaks, L_{IC}/L_S .

For FSRQs the synchrotron peak frequency is set based on the average peak frequency depicted in Figure 5 of Antón & Browne (2005) for the 1 Jy sample. This gives an average FSRQ peak frequency of $10^{14.0}$ Hz. The IC peak frequency of FSRQs is set at 1 MeV in accordance with Ajello et al. (2009). To determine the ratio L_{IC}/L_S the literature was searched yielding the spectra of forty FSRQs shown in Table 1. In cases where multiple spectra are given for the same object, the spectra corresponding to the most quiescent state is considered. Most sources show ratios of $\log(L_{IC}/L_S) \approx 1.0$ to 2.0 with a few sources showing ratios as low as $\log(L_{IC}/L_S) \approx 0.0$ or as high as $\log(L_{IC}/L_S) \approx 3.0$. The mode value for the ratio $\log(L_{IC}/L_S) = 1.0$ is used.

The BL Lac objects are divided into HBLs and LBLs assuming 10% of the BL Lac population are HBLs (Padovani et al. 2007). Similarly to the FSRQ subclass, the HBL and LBL synchrotron peak frequencies were assigned the average peak frequency from the Slew sample and 200mJy sample, respectively, as depicted in Figure 5 of Antón & Browne (2005). The average peak frequency is $10^{16.5}$ Hz for HBLs and $10^{14.5}$ Hz for LBLs. To set the IC peak frequency and IC peak luminosity for the HBL and LBL spectra, the ratios ν_{IC}/ν_S and L_{IC}/L_S from the SEDs modeled in the literature were consulted (see Table 2). All sources had $\log(\nu_{IC}/\nu_S) \approx 8.0$ to 9.0 and $\log(L_{IC}/L_S) \approx -1.5$ to 1.5. The mode values for the ratios were used, giving $\log(\nu_{IC}/\nu_S) = 8.0$ and $\log(L_{IC}/L_S) = 0.0$. Two LBLs were found to have complete spectrum models, BL Lacertae (Berger et al. 2008) and 3C 66A (Joshi & Böttcher 2007). The spectra of BL Lacertae and 3C 66A both have $\log(\nu_{IC}/\nu_S) \approx 7.0$ and $\log(L_{IC}/L_S) \approx 0.0$.

Figure 2 depicts the spectra used for FSRQs (solid lines) for $L_{151MHz} = 10^{43.0}$ erg s⁻¹, LBLs (dashed lines) for $L_{151MHz} = 10^{41.5}$ erg s⁻¹, and HBLs (dot-dashed lines) for $L_{151MHz} =$

$10^{40.0} \text{ erg s}^{-1}$.

2.2. AGN Contribution to the CXB

The non-blazar AGN contribution to the hard CXB is computed using standard synthesis modeling techniques (e.g., Comastri et al. 1995; Treister & Urry 2005; Ballantyne et al. 2006; Gilli et al. 2007). The fraction of Type 2 AGNs, f_2 , is assumed to be a function of both redshift and 2–10 keV luminosity, L_X : $f_2 \propto (1+z)^a (\log L_X)^{-b}$, with $a = 0.4$ (Ballantyne et al. 2006; Treister & Urry 2006) and $b = 4.7$. This evolution is normalized so that the non-blazar AGN type 2 to type 1 ratio is 4:1 at $z = 0$ and $\log L_X = 41.5$. The redshift evolution is halted at $z = 1$ in analogy with the evolution of the cosmic star-formation rate density (e.g., Ghandi & Fabian 2003; Hopkins & Beacom 2006).

AGNs with absorbing column densities less than $\log N_{\text{H}} = 22$ are considered to be unabsorbed type 1 sources, and they are distributed evenly over the following columns: $\log N_{\text{H}} = 20, 20.5, 21$ and 21.5 . Compton-thin Type 2 AGNs are also distributed equally over $\log N_{\text{H}} = 22, 22.5, 23$ and 23.5 . As current hard X-ray luminosity functions are missing Compton-thick AGNs, a parameter controlling the Compton thick fraction is defined, and any CT AGNs are distributed equally over $\log N_{\text{H}} = 24, 24.5$ and 25 . It is assumed that CT AGNs evolve in the same manner as less absorbed AGNs. The CT fraction, f_{CT} is defined to be the fraction of obscured AGN which are CT.

The unabsorbed rest-frame AGN spectrum consists of a power-law with photon index Γ and an exponential cutoff at energy E_{cut} , combined with a neutral reflection component calculated using the 'reflion' model within XSPEC (Ross & Fabian 2005). The strength of the reflection features in the total spectrum is typically parameterized by a reflection fraction, R , that is related to the covering factor of the reflector. Observationally, it is found that the strength of the reflection features decreases with luminosity, a relationship that is sometimes called the X-ray Baldwin effect (e.g., Bianchi et al. 2007). Therefore, we do not assume a constant value of R , rather the reflection spectrum is added to the power-law component such that the equivalent width of the Fe $K\alpha$ line agrees with the observed X-ray Baldwin effect found by Bianchi et al. (2007). In this way, the observed decrease in the strength of the reflection features with luminosity can be naturally included in the synthesis model. The relationship by Bianchi et al. (2007) gives an Fe $K\alpha$ equivalent width of 143 eV at $\log L_X = 41.5$, which is approximately equivalent to $R = 1.1$ for a $\Gamma = 1.9$ spectrum. The reflection fraction is proportional to the Fe $K\alpha$ EW, so R reduces to approximately 0.4 at $\log L_X = 44$ and 0.1 at $\log L_X = 47$. All the models presented here assume $E_{\text{cut}} = 250$ keV. Finally, following Gilli et al. (2007), spectra with $\Gamma = 1.5$ up to 2.3 are Gaussian averaged

around $\Gamma = 1.9$ to account for the observed dispersion in AGN spectral slopes. This results in a final rest-frame spectrum with luminosity L_X with the correct reflection strength.

2.3. AGN HXLFs

The AGN HXLFs considered are listed with their parameters in Table 3. Five of the HXLFs considered are LDDE models as proposed by Ueda et al. (2003). The Aird et al. (2009) HXLF considered is a LADE model. For the LDDE models, the luminosity function is described by the local luminosity function, $d\Phi(L_X, z = 0)/d \log L_X$ and an evolution factor $e(z, L_X)$, such that

$$\frac{d\Phi(L_X, z)}{d \log L_X} = \frac{d\Phi(L_X, 0)}{d \log L_X} e(z, L_X). \quad (9)$$

The local luminosity function is of the form

$$\frac{d\Phi(L_X, 0)}{d \log L_X} = A \left[\left(\frac{L_X}{L_*} \right)^{\gamma_1} + \left(\frac{L_X}{L_*} \right)^{\gamma_2} \right]^{-1}. \quad (10)$$

And the evolution factor is given by

$$e(z, L_X) = \begin{cases} (1+z)^{p_1} & z < z_c(L_x) \\ e(z_c) \left[\frac{1+z}{1+z_c(L_x)} \right]^{p_2} & z \geq z_c(L_x) \end{cases} \quad (11)$$

where

$$z_c(L_X) = \begin{cases} z_c^* & L_X \geq L_a \\ z_c^* \left(\frac{L_X}{L_a} \right)^\alpha & L_X < L_a \end{cases}. \quad (12)$$

The LADE model takes the same form as the LDDE local luminosity function defined in equation 10 and L_* and A are allowed to evolve with redshift such that

$$\log L_*(z) = \log L_0 - \log \left[\left(\frac{1.0 + z_c}{1.0 + z} \right)^{p_1} + \left(\frac{1.0 + z_c}{1.0 + z} \right)^{p_2} \right] \quad (13)$$

and

$$\log A(z) = \log A_0 + \alpha(1+z). \quad (14)$$

3. Results

3.1. Blazar contribution to the CXB

Figure 3 shows the calculated blazar and AGN contribution to the CXB and γ -ray background. The dotted line shows the AGN contribution to the CXB assuming the HXLF

presented by Ueda et al. (2003) and $f_{CT} = 0.5$. The dashed line is the FSRQ contribution while the dot-dashed line shows the BL Lac contribution. The BL Lacs are found to contribute greater than 100% of the γ -ray background. The possibility that the overestimation was due to inappropriate beaming parameters was investigated. Hovatta et al. (2009) found that BL Lacs tend to have Lorentz factors of $1.0 \leq \gamma \leq 38$. When this range of Lorentz factors is used and the BL Lac beaming parameters are set so that the average Lorentz factor is 10.3 and the average viewing angle is 5.3° , in agreement with Hovatta et al. (2009), the model overpredicts the γ -ray background by a factor of ~ 200 .

We have assumed that all radio galaxies viewed in the appropriate orientation are blazars. However, evidence suggests that AGNs, specifically radio galaxies, are an intermittent phenomenon (Burns et al. 1983; Cavaliere & Padovani 1989; Roettiger et al. 1993; Franceschini et al. 1998; Schoenmakers et al. 1999, 2000; Venturi et al. 2004; Jamrozy et al. 2007; Parma et al. 2007). BL Lac high energy radiation is primarily produced through synchrotron self-Compton (SSC) upscattering, since BL Lac jets propagate through regions with very little external radiation (Ghisellini et al. 2009a). For BL Lacs to emit high energy radiation, processes within the jet must accelerate electrons to relativistic speeds such that the electrons have enough energy to create synchrotron photons and then upscatter those photons. Therefore the high energy IC component of BL Lac jets would perhaps only be significant during infrequent events that cause rapid acceleration of electrons to high energies. Indeed, Giommi et al. (2006) found that unless BL Lacs have a small duty cycle the predicted blazar γ -ray emission would over predict the γ -ray background. The blazar and AGN contribution to the CXB assuming an X-ray duty cycle of 13% for BL Lacs, as shown in Figure 4, fits the data well. The BL Lac number counts predicted by this model in the 15-55 keV band are shown in Figure 5 with the BL Lac number counts observed by Ajello et al. (2009). The number counts predicted by this work are slightly larger but within a factor of 2.5 of the observations by Ajello et al. (2009).

More powerful sources, like FSRQs, are believed to accrete more efficiently and at a higher rate than low luminosity sources (Ho 2008). Bauer et al. (2009) studied variability in Palomar-QUEST survey blazars and found evidence that FSRQ duty cycles are greater than BL Lac duty cycles. No duty cycle for FSRQs is accounted for here, and indeed the background due to FSRQs is in reasonable agreement with that found by Ajello et al. (2009).

In the soft X-ray band (0.5-2 keV) the blazar contribution is found to be $\sim 12\%$, in agreement with the prediction of 11-12% by Giommi et al. (2006). The blazar contribution in the hard X-ray band (2-10 keV) is found to be $\sim 7.4\%$, in rough agreement with the prediction of $\sim 10\%$ by Ajello et al. (2009). In the 15.0-55.0 keV range blazars contribute $\sim 8.9\%$ of the X-ray background, in good agreement with the prediction of two distinct blazar classes by

Ajello et al. (2009) of $\sim 9\%$. Emissions from BL Lacs is found to account for the MeV background, in agreement with previous works (Giommi et al. 2006; Narumoto & Totani 2006; Kneiske & Mannheim 2008).

3.2. Implications for CT AGN

When the contribution of blazars to the CXB is properly considered, fewer CT AGN are required. In Figure 4 the AGN contribution to the CXB, as given by Ueda et al. (2003), is shown with $f_{CT} = 0.4$, in contrast to the canonical $f_{CT} = 0.5$. The CT fraction, f_{CT} required to appropriately model the peak of the CXB is shown for various HXLFs in Table 4 as well as the f_{CT} needed if the contribution of blazars is not considered. There is a $\sim 10\%$ uncertainty in the peak intensity of the CXB (e.g. HEAO-1 vs *Swift*). For the purposes of this work we assume $EF_E \approx 44.2 \text{ keV cm}^{-2} \text{ s}^{-1} \text{ str}^{-1}$ at 30 keV. Note that the estimated CT AGN fraction strongly depends on the CXB peak intensity adopted in the model. The Yencho and Silverman HXLFs depend heavily on CT sources to match the peak of the CXB; therefore, when blazars are considered the CT AGN fraction is still quite high. The number density of CT AGN at $z = 0$ with $L_X > 10^{43} \text{ erg s}^{-1}$ is also shown in Table 4 for the case of no blazar contribution to the CXB and for the case of blazar contribution to the CXB as described here. The number density as a function of redshift of CT AGN with $L_X > 10^{43} \text{ erg s}^{-1}$ needed to model the peak of the CXB for the HXLF given by Ueda et al. (2003) (solid lines) and Ebrero et al. (2009) (dashed lines) are shown in Figure 6. The thin black lines are the case where the blazar contribution to the CXB is not taken into account. The thick blue lines show the case where blazars are considered. The CT AGN density is reduced by a factor of 1.7 for the Ueda HXLF and a factor of 3.0 for the Ebrero HXLF. The AGN luminosity functions proposed by Silverman et al. (2008) and Yencho et al. (2009) require CT fractions where the majority of obscured AGN are CT. The AGN luminosity functions proposed by Ueda et al. (2003), La Franca et al. (2005), and Ebrero et al. (2009) require less than half the obscured AGN are CT, in agreement with Malizia et al. (2009) and Treister et al. (2009).

4. Discussion and Summary

It is clear that blazars make a non-negligible contribution to the CXB and significantly reduce the number of CT AGN predicted, and may be primarily responsible for the MeV background. This paper presents an upper limit to blazar contribution to the CXB by utilizing the unified model of radio-loud AGN. The main conclusions found here do not

change with a different choice of AGN radio luminosity function (e.g., Condon et al. 2002; Sadler et al. 2002; Best et al. 2005; Kaiser & Best 2007; Mauch & Sadler 2007); however, beaming parameters need to be modified as these luminosity functions do not distinguish between FRIs and FRIIs or high and low luminosity sources.

A recent study by Ajello et al. (2009), using the three year sample of *Swift*/BAT blazars, finds similar results for FSRQs as those found here; however, this work finds a greater contribution to the CXB and cosmic γ -ray background by BL Lacs. Due to the small number statistics and small redshift range of the *Swift*/BAT BL Lac sample, Ajello et al. (2009) are not able to uniquely determine the evolutionary parameters and thus assume no evolution for BL Lacs. This work assumes BL Lacs evolve in the same manner as low luminosity radio galaxies. Also, Ajello et al. (2009) assume a simple power law SED model for BL Lacs whereas this work utilizes an SED model based on average BL Lac properties taking into account the variety of BL Lac subclasses of LBLs and HBLs. Several studies have found that BL Lacs contribute substantially to the cosmic γ -ray background (Giommi et al. 2006; Narumoto & Totani 2006; Kneiske & Mannheim 2008), thus it is not expected that the BL Lac contribution to the CXB is negligible, as found by Ajello et al. (2009). As this work uses a more physical BL Lac SED model and a reasonable evolutionary model, we expect that this work may more accurately model the BL Lac contribution to the CXB, although the factor 2.5 discrepancy in the BL Lac source counts in the hard X-ray band must be solved in future works.

Treister et al. (2009) find the density of CT AGN at $z = 0$ with $L_X > 10^{43}$ erg s $^{-1}$ is $\sim 2.2 \times 10^{-6}$ Mpc $^{-3}$. The luminosity function of Ueda et al. (2003) predicts the density of CT AGN with $L_X > 10^{43}$ erg s $^{-1}$ at $z = 0$ to be 7.3×10^{-6} Mpc $^{-3}$ if blazars are not considered and 4.4×10^{-6} Mpc $^{-3}$ if blazars are considered. With the blazar contribution to the CXB considered, the Ueda et al. (2003) over predicts the CT AGN density found by Treister et al. (2009), by a factor of 2. Conversely, the luminosity function proposed by Ebrero et al. (2009) predicts the density of CT AGN with $L_X > 10^{43}$ erg s $^{-1}$ at $z = 0$ to be 1.1×10^{-6} Mpc $^{-3}$ if blazars are not considered and 3.6×10^{-7} Mpc $^{-3}$ if blazars are considered, which is a factor of 6 smaller than the density reported by Treister et al. (2009). According to the INTEGRAL results of Malizia et al. (2009), the $f_{CT} \geq 0.32$ with no upper limit given. Between different HXLFs there is a large scatter in the predicted f_{CT} and the predicted CT AGN density varies by a factor of 30. This clearly illustrates the limits imposed by the uncertainty of the low luminosity end of the AGN HXLF and how important it is for future missions to probe this portion of the HXLF.

It has been shown that blazars, specifically BL Lacs, contribute the majority of the γ -ray background (Giommi et al. 2006; Narumoto & Totani 2006; Kneiske & Mannheim 2008).

Giommi et al. (2006) found that unless BL Lacs have a small high energy duty cycle the predicted blazar γ -ray emission would over predict the γ -ray background. Furthermore, Kneiske & Mannheim (2008) suggests that using radio blazar luminosity functions may cause an overestimation of the number of sources emitting robustly at higher energies, as it is not certain that all radio sources will have strong X-ray and γ -ray emission. Physical and evolutionary models of quasars indicate that AGN activity is short-lived and possibly recurrent (Soltan 1982; Cavaliere & Padovani 1989; Chokshi & Turner 1992). Franceschini et al. (1998) showed that long-lived, continuous AGN activity is not consistent with the black hole mass function they calculated from their sample of 13 local galaxies, but short-lived and recurrent AGN activity matches the data well. Several sources which appear to be restarted AGNs have been observed (Burns et al. 1983; Roettiger et al. 1993; Schoenmakers et al. 1999; Venturi et al. 2004; Jamrozy et al. 2007; Fabian et al. 2009). Sources have also been observed which have relic radio lobes but the AGN activity is not currently in an active phase (Parma et al. 2007; Dwarakanath & Kale 2009; Fabian et al. 2009). Recent observations by *Hubble Space Telescope* and *Chandra* of the relativistic jet of nearby M87 provide evidence for the intermittent nature of jet X-ray emission (e.g., Perlman et al. 2003; Harris et al. 2006; Stawarz et al. 2006; Madrid 2009). Large amplitude flaring has been observed from the previously quiescent knot HST-1 in the jet of M87 since 2000 (Madrid 2009). This flaring activity is shown to be consistent with shocks occurring within the jet as faster moving particles collide with slower relativistic particles injected into the jet at an earlier time (Perlman et al. 2003; Stawarz et al. 2006; Madrid 2009). Perlman et al. (2003) and Stawarz et al. (2006) suggest the recent X-ray flaring of HST-1 is directly related to material injected at the base of the jet 30-40 years ago. Therefore, a jet X-ray duty cycle is expected.

Finally, due to the spectral steepening that occurs after the flow of energetic particles into the jet has ceased, the best frequency range to search for relic radio lobes is the low radio regime, less than 1 GHz (Parma et al. 2007). Therefore, it is likely that the radio AGN luminosity function given by Willott et al. (2001) at 151 MHz includes relic radio lobes. As this would affect the low luminosity end of the luminosity function more prevalently as relic sources tend to not be as luminous as active sources (Dwarakanath & Kale 2009), the BL Lac luminosity function found here may overpredict the number of BL Lacs. Thus, the average BL Lac X-ray duty cycle is likely to be somewhat larger than the 13% found here.

The authors thank C.M. Pierce for reviewing a draft of this paper and the referee for helpful comments.

A. Blazar Spectrum Parametrization

The synchrotron and IC contributions to the SED are both parametrized in $\log(\nu) - \log(L)$ space by a linear curve which transitions to a parabolic curve, parametrized by the 151 MHz luminosity, L_{151MHz} (Fossati et al. 1997, 1998; Donato et al. 2001). For $x = \log \nu$, $x_R = \log(151 \text{ MHz})$, $x_X = \log(1 \text{ keV}/h_p)$, where h_p is Planck's constant, $\psi(x) = \log L(\log \nu)$, $\psi_R = \log L_{151MHz}$, and $\psi_X = \log L_{1keV}$, $L(\nu)$ can be found by

$$\psi(x) = \log(10^{\psi_S} + 10^{\psi_{IC}}) \quad (\text{A1})$$

where

$$\psi_S = \begin{cases} (1 - \alpha_s)(x - x_R) + \psi_R & x \leq x_{trs} \\ -[(x - x_s)/\sigma]^2 + \psi_{sp} & x > x_{trs} \end{cases} \quad (\text{A2})$$

and

$$\psi_{IC} = \begin{cases} (1 - \alpha_c)(x - x_X) + \psi_X & x \leq x_{trc} \\ -[(x - x_c)/\sigma]^2 + \psi_{cp} & x > x_{trc} \end{cases}. \quad (\text{A3})$$

Fossati et al. (1997) gives the synchrotron slope $\alpha_s = 0.2$, the synchrotron transitional frequency $\nu_{trs} = 5 \times 10^{10}$ Hz, and the width parameter

$$\sigma = \left[-\frac{x_{trs} - x_s}{1 - \alpha_s} \right]^{1/2}, \quad (\text{A4})$$

while Donato et al. (2001) gives the inverse Compton peak slope $\alpha_c = 0.6$.

To ensure continuity of ψ_S at x_{trs} , the parameter ψ_{sp} is defined

$$\psi_{sp} \equiv (1 - \alpha_s)(x_{trs} - x_R) + \left[\frac{x_{trs} - x_s}{\sigma} \right]^2 + \psi_R. \quad (\text{A5})$$

For ψ_{IC} to be continuous and differentiable at x_{trc} , ψ_X must be defined as

$$\psi_X \equiv - \left[\frac{x_{trc} - x_c}{\sigma} \right]^2 - (1 - \alpha_c)(x_{trc} - x_X) + \psi_{cp} \quad (\text{A6})$$

and the transition frequency between the linear and parabolic portion of ψ_{IC} , ν_{trc} , must be defined such that

$$x_{trc} \equiv x_c - \sigma^2(1 - \alpha_c)/2. \quad (\text{A7})$$

In §2.1.3 the synchrotron peak frequency $\nu_S = 10^{x_S}$, the ratio between the inverse Compton and synchrotron peak frequencies $\nu_{IC}/\nu_S = x_c - x_s$, and the ratio between the inverse Compton and synchrotron peak luminosities $L_{IC}/L_S = \psi_{cp} - \psi_{sp}$ are set according to observational data and individual blazar SED models.

REFERENCES

- Abdo, A.A., et al.2009, ApJS, 183, 46
- Aharonian, F., et al.2008, A&A, 481, L103
- Aird, J., et al.2009, MNRAS, in press (arXiv: 0910:1141)
- Ajello, M., et al.2008, ApJ, 689, 666
- Ajello, M. et al.2009, ApJ, 699, 603
- Alexander, D.M., et al.2003, AJ, 126, 539
- Antón, S. & Browne, I.W.A. 2005, MNRAS, 356, 225
- Antonucci, R. 1993, ARA&A, 31, 473
- Ballantyne, D.R., Everett, J.E., Murray, N. 2006, ApJ, 639, 740
- Ballantyne, D.R. & Papovich, C. 2007, ApJ, 660, 988
- Barger, A.J., Cowie, L.L., Mushotzky, R.F., Yang, Y., Wang, W.-H., Steffen, A.T., & Capak, P. 2005, AJ, 129, 578
- Bauer, A., Baltay, C., Coppi, P., Ellman, N., Jerke, J., Rabinowitz, D., & Scalzo, R. 2009, ApJ, 699, 1732
- Berger, K., Wagner, R.M., Hayashida, M., Kranich, D., Lindfors, E., Lorenz, E., Vitale, V. 2008, in AIP Conf. Proc. Vol. 1085, High Energy Gamma-Ray Astronomy, ed. F.A. Aharonian, W. Hofmann, & F. Reiger (Heidelberg: AIP), 467
- Best, P.N., Kauffmann, G., Heckman, T.M., & Ivezić, Ž. 2005, MNRAS, 362, 9
- Bianchi, S., Guainazzi, M., Matt, G. & Fonseca Bonilla, N. 2007, A&A, 467, L19
- Bianchin, V. et al.2009, A&A, 496, 423
- Brandt, W.N. & Hasinger, G. 2005, ARA&A, 43, 827
- Burns, J.O., Schwendeman, E., & White, R.A. 1983 ApJ, 271, 575
- Caccianiga, A. & Marchã, M.J.M. 2004, MNRAS, 348, 937
- Cavaliere, A. & Padovani, P. 1989, ApJ, 340, L5

- Celotti, A., Fabian, A.C., & Rees, M.J. 1992, MNRAS, 255, 419
- Chokshi, A. & Turner, E.L. 1992, MNRAS, 259, 421
- Churazov, E., et al.2007, A&A, 467, 529
- Comastri, A., Setti, G., Zamorani, G., & Hasinger G. 1995, A&A, 296, 1
- Condon, J.J., Cotton, W.D., & Broderick, J.J. 2002, AJ, 124, 675
- Costamante, L., Aharonian, F., Bühler, R., Khangulyan, D., Reimer, A., & Reimer, O. 2008, in AIP Conf. Proc. Vol. 1085, High Energy Gamma-Ray Astronomy, ed. F.A. Aharonian, W. Hofmann, & F. Reiger (Heidelberg:AIP), 644
- Cowie, L.L., Songaila, A., & Barger, A.J. 1999, ApJ, 118, 603
- De Luca, A. & Molendi, S. 2004, A&A, 419, 837
- Donato, D., Ghisellini, G., Tagliaferri, G., Fossati, G. 2001, A&A, 375, 739
- Dwarakanath, K.S. & Kale, R. 2009, ApJ, 698, L163
- Ebrero, J., et al.2009, A&A, 493, 55
- Fabian, A.C. & Barcons, X. 1992, ARA&A, 30, 429
- Fabian, A.C., Chapman, S., Casey, C.M., Bauer, F. & Blundell, K.M. 2009, MNRAS, 395, L67
- Ferrarese, L. & Merritt, D. 2000, ApJ, 539, L9
- Fiore, F., La Franca, F., Giommi, P., Elvis, M., Matt, G., Comastri, A., Molendi, S., & Gioia, I. 1999, MNRAS, 306, L55
- Foschini, L., et al.2006, A&A, 453, 829
- Fossati, G., Celotti, A., Ghisellini, G., & Maraschi, L. 1997, MNRAS, 289, 136
- Fossati, G., Maraschi, L., Celotti, A., Comastri, A., & Ghisellini, G. 1998, MNRAS, 299, 433
- Franceschini, A., Vercellone, S., & Fabian, A.C. 1998, MNRAS, 297, 817
- Gendreau, K.C., et al.1995, PASJ, 47, L5
- Gandhi, P. & Fabian, A.C., 2003, MNRAS, 339, 1095

- Ghisellini, G., Haardt, R., & Matt, G. 1994, MNRAS, 267, 743
- Ghisellini, G., Celotti, A., Fossati, G., Maraschi, L., & Comastri, A. 1998, MNRAS, 301, 451
- Ghisellini, G. & Tavecchio, F. 2008, MNRAS, 387, 1669
- Ghisellini, G., Maraschi, L., & Tavecchio, F. 2009a, MNRAS, 396, L105
- Ghisellini, G., Tavecchio, F., & Ghirlanda, G. 2009b, MNRAS, submitted (arXiv: 0906.2195)
- Giacconi, R., Gursky, H., Paolini, F.R., & Rossi, B.B. 1962, Phys. Rev. Lett., 9, 439
- Giacconi, R., et al.2001, ApJ, 551, 624
- Giacconi, R., et al.2002, ApJS, 139, 369
- Gilli, R., Comastri, A. & Hasinger, G. 2007, A&A, 463, 79
- Giommi, P., Colafrancesco, S., Cavazzuti, E., Perri, M., & Pittori, C. 2006, A&A, 445, 843
- Giuliani, A., et al.2009, A&A, 494, 509
- Gruber, D.E., Matteson, J.L., Peterson, L.E. & Jung, G.V. 1999, ApJ, 520, 124
- Guainazzi, M., Matt, G., & Perola, G.C. 2005, A&A, 444, 119
- Harris, D.E., Cheung, C.C., Biretta, J.A., Sparks, W.B., Junor, W., Perlamm, E.S., & Wilson, A.S. 2006, ApJ, 640, 211
- Hasinger, G., Burg, R., Giacconi, R., Schmidt, M., Trumper, J., & Zamorani, G. 1998, A&A, 329, 482
- Hasinger, G., et al.2001, A&A, 365, L45
- Hasinger, G., Miyaji, T., & Schmidt, M. 2005, A&A, 441, 417
- Ho, L.C. 2008, ARA&A, 46, 475
- Hopkins, A.M. & Beacom, J.F. 2006, ApJ, 651, 142
- Hovatta, T., Valtaoja, E., Tornikoski, M., & Lähteenmäki, A. 2009, A&A, 494, 527
- Jamrozy, M., Konar, C., Saikia, D.J., Stawarz, L., Mack, K.-H., & Siemiginowska, A. 2007, MNRAS, 378, 581

- Joshi, M. & Böttcher, M. 2007, ApJ, 662, 884
- Kaiser, C.R. & Best, P.N. 2007, MNRAS, 381, 1548
- Kneiske, T.M. & Mannheim, K. 2008, A&A, 479, 41
- Kushino, A., Ishisaki, Y., Morita, U., Yamasaki, N.Y., Ishida, M., Ohashi, T. & Ueda, Y. 2002, PASJ, 54, 327
- La Franca, F. et al. 2005, ApJ, 635, 864
- Lumb, D.H., Warwick, R.S., Page, M. & De Luca, A. 2002, A&A, 389, 93
- Lynden-Bell, D. 1969, Nature, 223, 690
- Madau, P., Ghisellini, G., & Fabian, A.C. 1994, MNRAS, 270, L17
- Madrid, J.P. 2009, AJ, 137, 3864
- Malizia, A., Stephen, J.B., Bassani, L., Bird, A.J., Panessa, F., & Ubertini, P. 2009, MNRAS, in press (arXiv: 0906.5544)
- Maraschi, L., Foschini, L., Ghisellini, G., Tavecchio, F., & Sambruna, R.M. 2008, MNRAS, 391, 1981
- Massaro, E., Tramacere, A., Perri, M., Giommi, P., & Tosti, G. 2006, A&A, 448, 861
- Mauch, T. & Sadler, E.M. 2007, MNRAS, 375, 931
- Mushotzky, R.F., Cowie, L.L., Barger, A.J., & Arnaud, K.A. 2000, Nature, 404, 459
- Narumoto, T. & Totani, T. 2006, ApJ, 643, 81
- Nieppola, E., Valtaoja, E., Tornikoski, M., Hovatta, T., & Kotiranta, M. 2008, A&A, 488, 867
- Padovani, P. 2007, Ap&SS, 309, 63
- Padovani, P., Giommi, P., Landt, H., Perlman, E.S. 2007, ApJ, 662, 182
- Padovani, P. & Urry, C.M. 1992, ApJ, 387, 449
- Parma, P., Murgia, M., de Ruiter, H.R., Fanti, R., Mack, K.-H., & Govoni, F. 2007, A&A, 470, 875

- Perlman, E.S., Harris, D.E., Biretta, J.A., Sparks, W.B., & Macchetto, F.D. 2003, *ApJ*, 599, L65
- Pompilio, F., La Franca, F., & Matt, G. 2000, *A&A*, 353, 440
- Rees, M.J. 1984, *ARA&A*, 22, 471
- Revnivtsev, M., Gilfanov, M., Sunyaev, R., Jahoda, K. & Markwardt, C. 2003, *A&A*, 411, 329
- Risaliti, G., Maiolino, R., & Salvati, M. 1999, *ApJ*, 522, 157
- Roettiger, K., Burns, J.O., Clarke, D.A., & Christiansen, W.A. 1993, *BAAS*, 25, 1444
- Ross, R.R. & Fabian, A.C. 2005, *MNRAS*, 358, 211
- Sadler, E.M., et al.2002, *MNRAS*, 329, 227
- Schoenmakers, A.P., de Bruyn, A.G., Rötgering, H.J.A., & van der Laan, H. 1999, *A&A*, 341, 44
- Schoenmakers, A.P., de Bruyn, A.G., Rötgering, H.J.A., van der Lann, H., & Kaiser, C.R. 2000, *MNRAS*, 315, 371
- Setti, G. & Woltjer, L. 1989, *A&A*, 224, L21
- Silverman, J.D., et al.2008, *ApJ*, 679, 118
- Smolčić, V. 2009, *ApJ*, 699, L43
- Smolčić, V., et al.2009, *ApJ*, 696, 24
- Sołtan, A. 1982, *MNRAS*, 200, 115
- Spergel, D.N., et al.2007, *ApJS*, 170, 377
- Sreekumar, P., et al.1998, *ApJ*, 494, 523
- Stawarz, Ł., Aharonian, F., Kataoka, J., Ostrowski, M., Siemiginowska, A., & Sikora, M. 2006, *MNRAS*, 370, 981
- Stecker, F.W., Hunter, S.D., & Kniffen, D.A. 2008, *Astropart. Phys.*, 29, 25
- Strong, A.W., Moskalenko, I.V., & Reimer, O. 2004, *ApJ*, 613, 956
- Tagliaferri, G. et al.2008, *ApJ*, 679, 1029

- Tavecchio, F., Maraschi, L., Ghisellini, G., Kataoka, J., Foschini, L., Sambruna, R.M., & Tagliaferri, G. 2007, *ApJ*, 665, 980
- Treister, E. & Urry, C.M. 2005, *ApJ*, 630, 115
- Treister, E. & Urry, C.M. 2006, *ApJ*, 652, L79
- Treister, E., Urry, C.M., & Virani, S. 2009, *ApJ*, 696, 110
- Ueda, Y., Akiyama, M., Ohta, K., & Miyaji, T. 2003, *ApJ*, 598, 886
- Urry, C.M. 1999, in *ASP Conf Ser. 159, BL Lac Phenomenon*, ed. L.O. Takalo & A. Sillanpää (Turku: ASP), 3
- Urry, C.M. & Padovani, P. 1991 *ApJ*, 371, 60
- Urry, C.M. & Padovani, P. 1995, *PASP*, 107, 803
- Urry, C.M., Padovani, P., & Stickel, M. 1991, *ApJ*, 382, 501
- Urry, C.M. & Shafer, R.A. 1984, *ApJ*, 280, 569
- Vecchi, A., Molendi, S., Guainazzi, M., Fiore, F. & Parmar, A. 1999, *A&A*, 349, L73
- Venturi, T., Dallacasa, D., & Stefanachi, F. 2004, *A&A*, 422, 515
- Vercellone, S., et al. 2009, in *AIP Conf. Proc. Vol. 1112, Science With the New Generation of High Energy Gamma-ray Experiments*, ed. D. Bastieri & R. Rando (Abano Terme:AIP), 121
- Watanabe, K., Hartmann, D.H., Leising, M.D., & The, L.-S. 1999, *ApJ*, 516, 285
- Watanabe, S., et al. 2009, *ApJ*, 694, 294
- Weidenspointner, G., et al. 2000, in *AIP Conf. Proc. Vol. 510, The Fifth Compton Symposium*, ed. M.L. McConnell & J.M. Ryan (Portsmouth, NH: AIP), 467
- Willott, C.J., Rawlings, S., Blundell, K.M., Lacy, M. & Eales, S.A. 2001, *MNRAS*, 322, 536
- Worsley, M., Fabian, A.C., Barcons, X., Mateos, S., Hasinger, G., & Brunner, H. 2004, *MNRAS*, 352, L28
- Worsley, M., et al. 2005, *MNRAS*, 357, 1281
- Yencho, B., Barger, A.J., Trouille, L., & Winter, L.M. 2009, *ApJ*, 698, 380

Table 1. FSRQs used for determining L_{IC}/L_S . Sources used in table: F06 Foschini et al. (2006), T07 Tavecchio et al. (2007), M08 Maraschi et al. (2008), B09 Bianchin et al. (2009), Gi09 Giuliani et al. (2009), Gh09 Ghisellini et al. (2009b), V09 Vercellone et al. (2009), & W09 Watanabe et al. (2009).

Name	Source	$\approx \log(L_{IC}/L_S)$
RBS 315	T07	2.0
S5 0836+71	T07	2.0
J0746.3+2548	W09	1.5
PKS 2149-306	B09	1.0
3C 279	Gi09	1.0
3C 454.3	V09	1.0
2141.2+1730	M08	0.0
0521.7+7918	M08	0.0
1234.9+6651	M08	1.0
1050.9+5418	M08	0.5
0402.0-3613	M08	0.0
0828.7+6601	M08	1.0
1623.4+2712	M08	1.0
1340.7+2859	M08	1.0
0152.4+0424	M08	1.5
0232.5-0414	M08	0.0
SDSS J081009.94+384757	M08	1.5
MG3 J225155+2217	M08	3.0
0048-071	Gh09	1.5
0202-17	Gh09	1.5
0215-015	Gh09	0.0
0528+134	Gh09	2.0
2251-158	Gh09	1.0
0227-369	Gh09	2.0
0454-234	Gh09	1.0
0347-221	Gh09	2.0
0820+560	Gh09	1.5
0917+449	Gh09	1.0
1454-354	Gh09	1.0
1013-054	Gh09	1.5
1502+106	Gh09	1.0

Table 1—Continued

Name	Source	$\approx \log(L_{IC}/L_S)$
1329-049	Gh09	1.5
1520-319	Gh09	2.0
1551+130	Gh09	1.0
2052-447	Gh09	2.0
1633+382	Gh09	1.5
2227-088	Gh09	1.5
2023-077	Gh09	2.0
2325+093	Gh09	2.0
PKS 1334-127	F06	0.5

Table 2. HBLs used for determining L_{IC}/L_S and ν_{IC}/ν_S . Sources used in table: A08 Aharonian et al. (2008), C08 Costamante et al. (2008), M08 Maraschi et al. (2008), T08 Tagliaferri et al. (2008), G09 Ghisellini et al. (2009b), F06 Foschini et al. (2006), M06 Massaro et al. (2006).

Name	Source	$\approx \log(L_{IC}/L_S)$	$\approx \log(\nu_{IC}/\nu_S)$
RGB J0152+017	A08	0.0	8.0
PKS 2155-304	C08	0.0	9.0
J1456.0+5048	M08	0.0	9.0
1ES1959+650	T08	-1.5	8.0
0426-380	G09	1.5	8.0
0235+164	F06	0.0	8.0
Mkn 501	M06	0.0	8.0

Table 3. Parameters of AGN X-ray Luminosity Functions considered. ^a in units of h_{70}^3 Mpc^{-3} . ^b in units of h_{70}^{-2} erg s^{-1} . ^c an LADE model.

Luminosity Function	A/A_0^a	$\log L_*/\log L_0^b$	γ_1	γ_2	p_1	p_2	z_c^*/z_c	$\log L_a^b$	α
Ueda et al. (2003)	5.04e-6	43.94	0.86	2.23	4.23	-1.5	1.9	44.6	0.335
La Franca et al. (2005)	1.21e-6	44.25	1.01	2.38	4.62	-1.15	2.49	45.74	0.20
Silverman et al. (2008)	6.871e-7	44.33	1.10	2.15	4.22	-3.27	1.89	44.6	0.333
Ebrero et al. (2009)	4.78e-6	43.91	0.96	2.35	4.07	-1.5	1.9	44.6	0.245
Yenko et al. (2009)	7.24e-7	44.40	0.872	2.36	3.61	-2.83	2.18	45.09	0.208
Aird et al. (2009) ^c	2.95e-5	44.77	0.62	3.01	6.36	-0.24	0.75	-	-0.19

Table 4. f_{CT} needed for luminosity function to match the peak of the X-ray background and corresponding CT number density at $z = 0$ in Mpc^{-3} for $L_X > 10^{43}$ erg s^{-1}

Luminosity Function	f_{CT}		CT number density at $z = 0$ (Mpc^{-3})	
	Without Blazars	With Blazars	Without Blazars	With Blazars
Ueda et al. (2003)	0.5	0.4	7.3×10^{-6}	4.4×10^{-6}
La Franca et al. (2005)	0.3	0.2	2.0×10^{-6}	1.6×10^{-6}
Silverman et al. (2008)	0.8	0.8	1.4×10^{-5}	1.2×10^{-5}
Ebrero et al. (2009)	0.1	0.02	1.1×10^{-6}	3.6×10^{-7}
Yenko et al. (2009)	0.8	0.8	1.7×10^{-5}	1.6×10^{-5}
Aird et al. (2009)	0.7	0.6	5.2×10^{-6}	4.7×10^{-6}

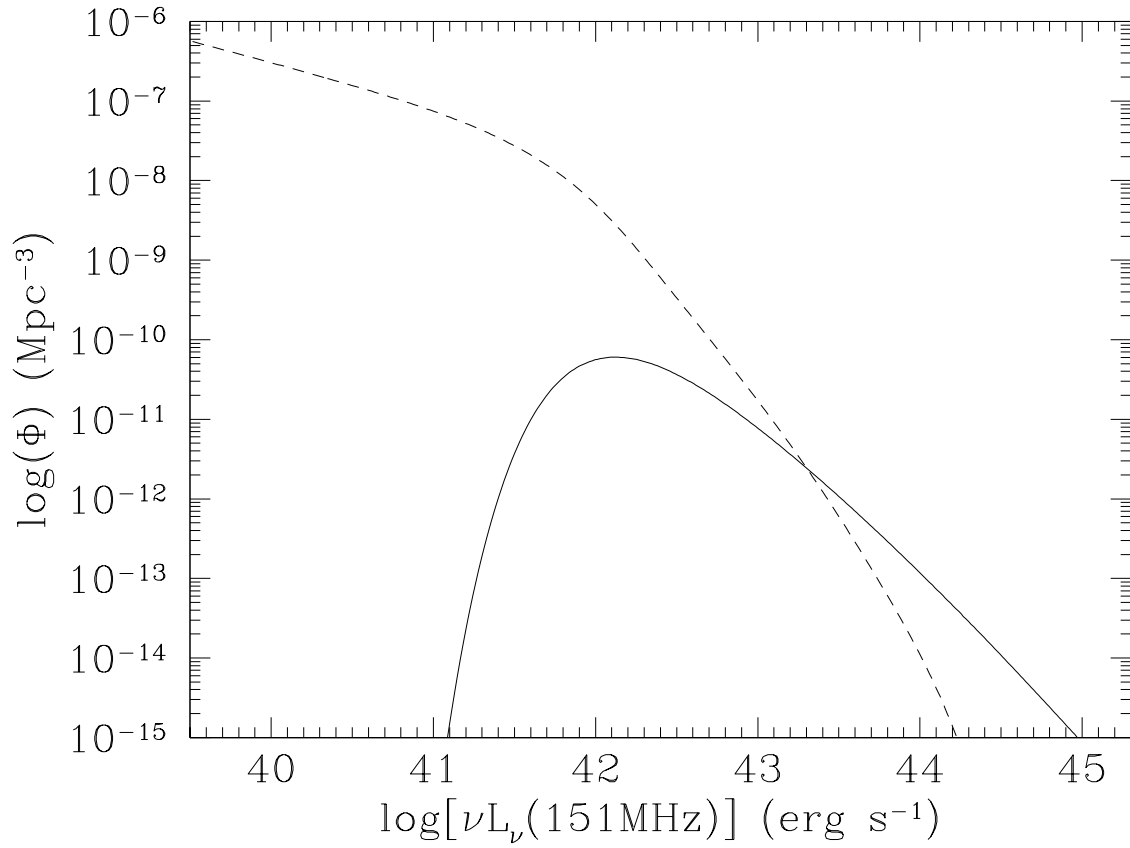


Fig. 1.— Rest frame radio AGN luminosity function by Willott et al. (2001) model C relativistically beamed using the method of Urry & Shafer (1984) and Urry & Padovani (1991) at $z = 1$ separated into FSRQs (solid line) and BL Lacs (dashed line).

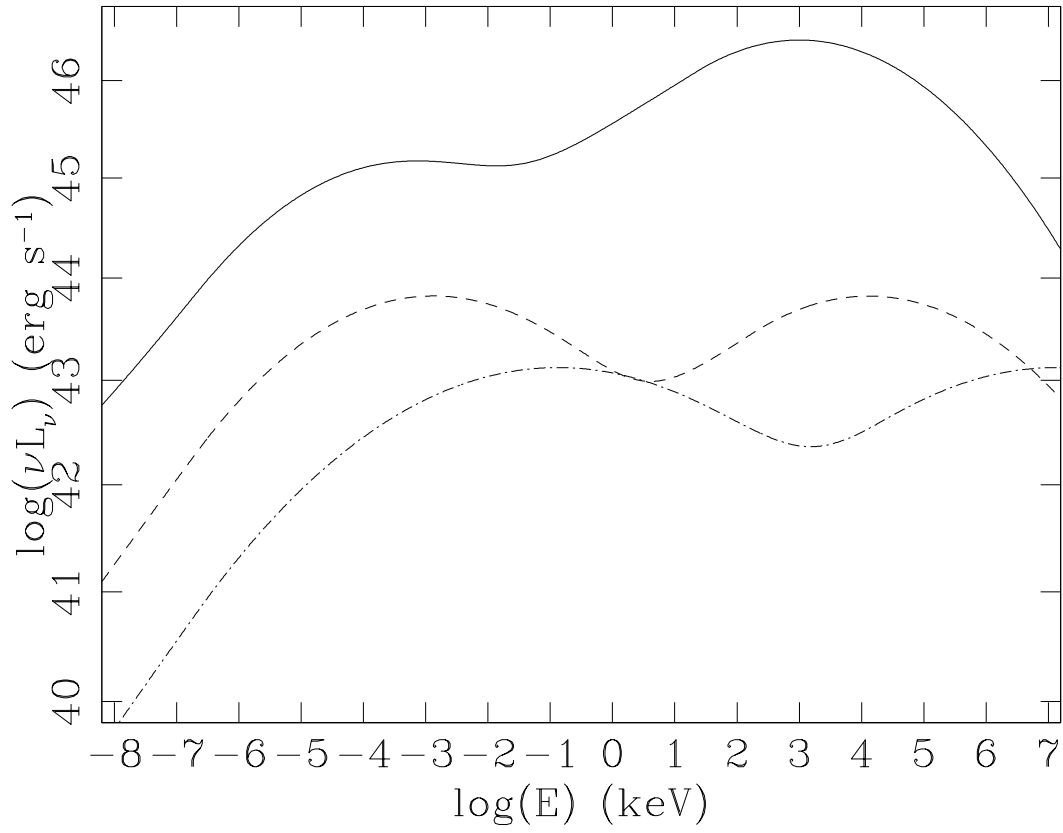


Fig. 2.— Rest frame spectral energy distributions used for FSRQ (solid line) with $\log \nu L_\nu(151$ MHz) $=43.0$, LBL (dashed line) with $\log \nu L_\nu(151$ MHz) $=41.5$, and HBL (dot-dashed line) with $\log \nu L_\nu(151$ MHz) $=40.0$.

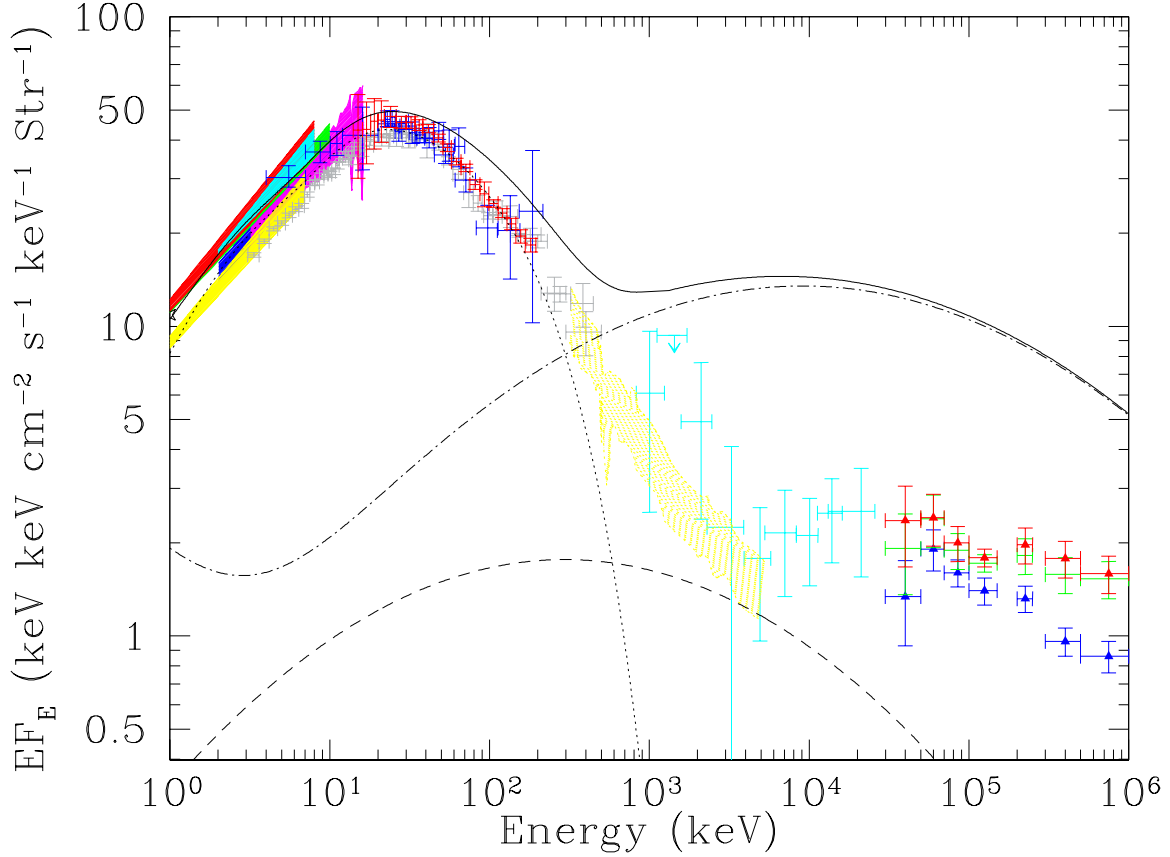


Fig. 3.— AGN and Blazar contribution (solid line) to the X-ray and γ -ray background if BL Lac duty cycle is 100%. AGN (dotted line- using Ueda et al. 2003 X-ray luminosity function and CT fraction $f_{ct} = 0.5$), FSRQs (dashed line), and BL Lacs (dot-dashed line). The colored data and areas denote measurements from various instruments: blue - ASCA GIS (Kushino et al. 2002); magenta - RXTE (Revnivtsev et al. 2003); green - XMM-Newton (Lumb et al. 2002); red - BeppoSAX (Vecchi et al. 1999); yellow - ASCA SIS (Gendreau et al. 1995); cyan - XMM-Newton (De Luca & Molendi 2004); light yellow - SMM (Watanabe et al. 1999); grey data - HEAO-1 (Gruber et al.1999); blue data - INTEGRAL (Churazov et al. 2007); red data - SWIFT BAT (Ajello et al. 2008); cyan data - COMPTEL (Weidenspointer et al. 2000); red triangles - EGRET (Sreekumar et al. 1998); blue triangles - reevaluation of EGRET (Strong et al. 2004); green data - renormalization of EGRET based Sreekumar et al. 1998 (Stecker et al. 2008).

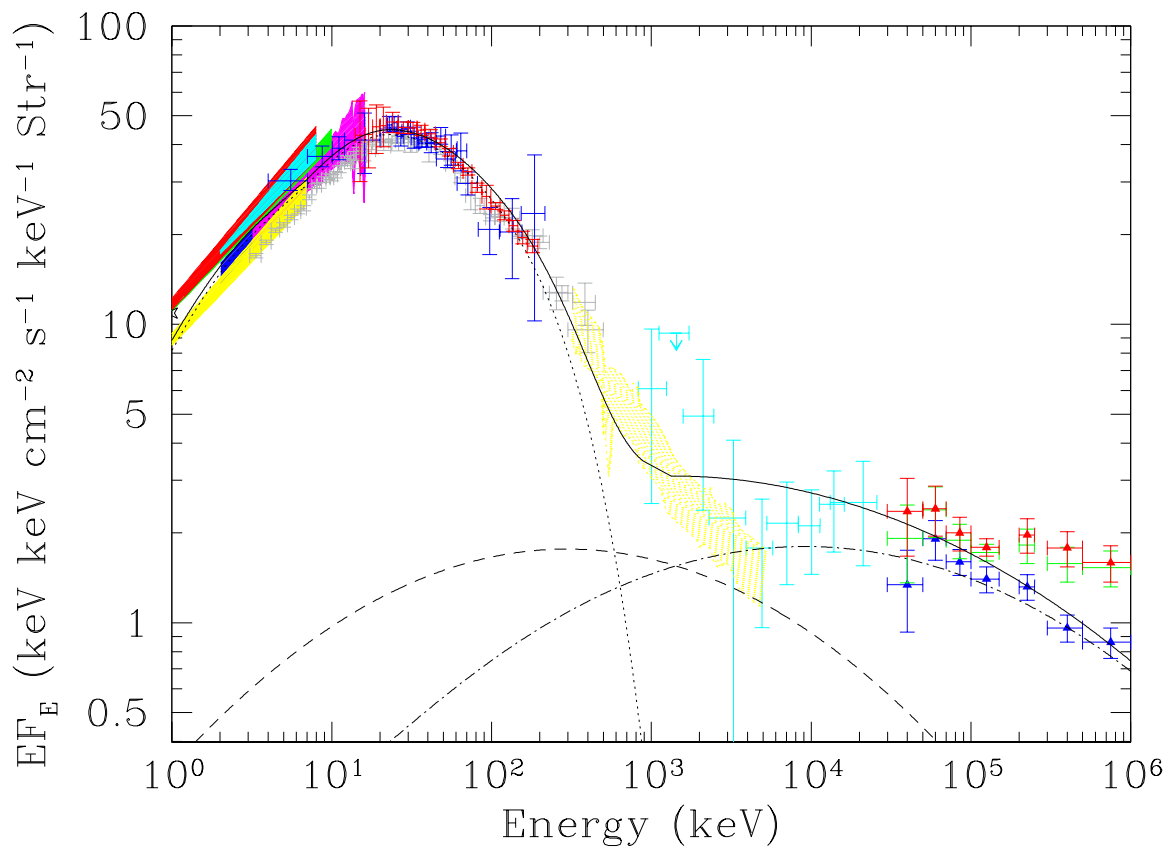


Fig. 4.— AGN and Blazar contribution (solid line) to the X-ray and γ -ray background. AGN (dotted line- using Ueda et al. 2003 X-ray luminosity function and CT fraction $f_{ct} = 0.4$), FSRQs (dashed line), and BL Lacs (dot-dashed line) with an X-ray duty cycle of 13%. Data the same as in Figure 3.

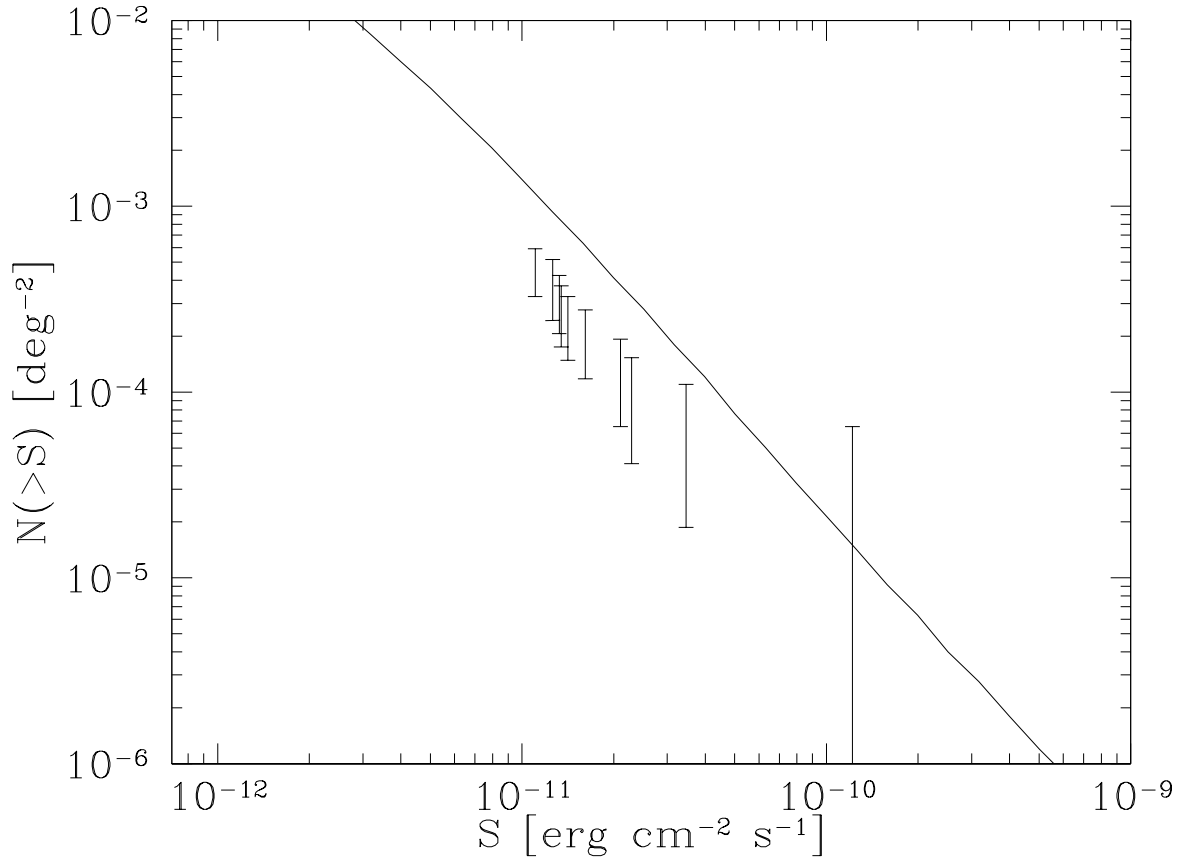


Fig. 5.— BL Lac number density counts for 15-55 keV band assuming an X-ray duty cycle of 13%. Data shown from Ajello et al. (2009) Figure 12b.

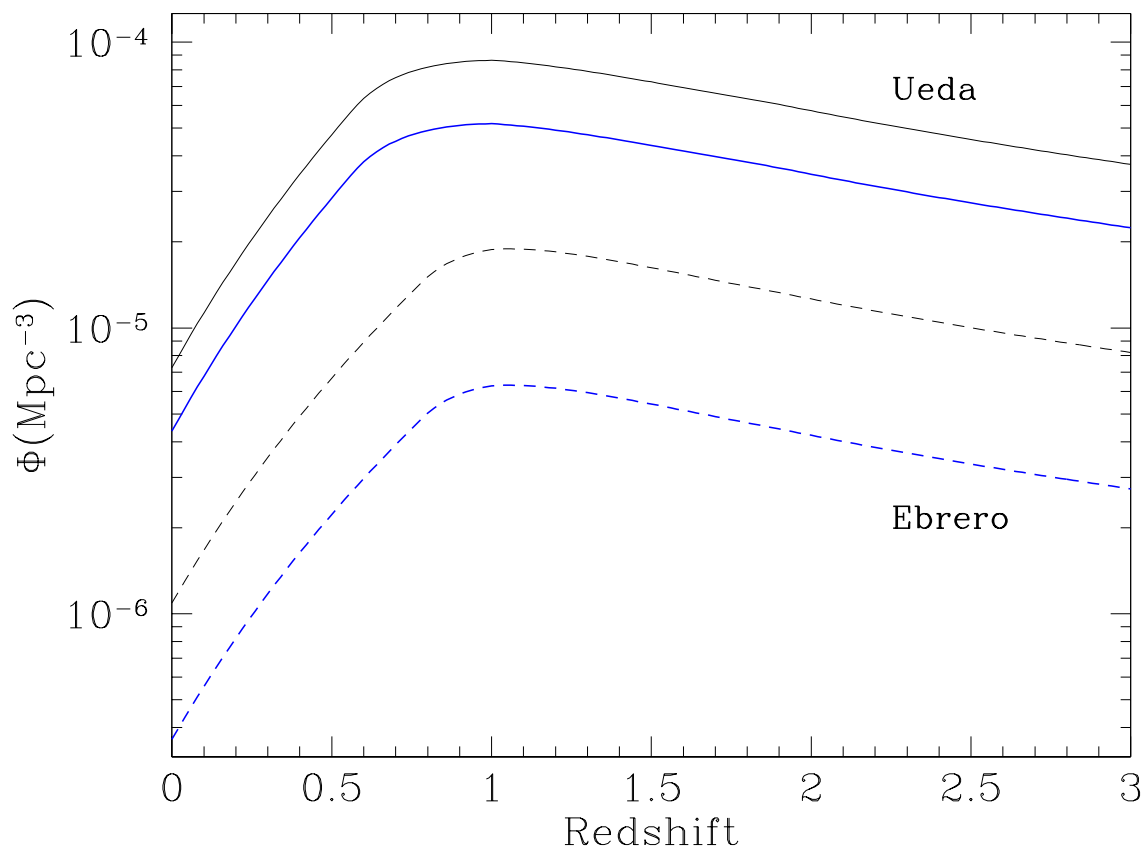


Fig. 6.— Number density of CT AGN with $L_X > 10^{43}$ erg s $^{-1}$ as a function of redshift for the HXLFs given by Ueda et al. (2003) (solid lines) and Ebrero et al. (2009) (dashed lines). The black(thin) lines are the CT AGN needed if blazars are not considered. The blue(thick) lines are the CT AGN needed if the blazar contribution to the CXB is considered.